Journal of Energy Storage 16 (2018) 250–258

Contents lists available at ScienceDirect

Journal of Energy Storage

journal homepage: www.elsevier.com/locate/est

DERs integration in microgrids using VSCs via proportional feedback linearization control: Supercapacitors and distributed generators

Oscar Danilo Montoya[a,*], Alejandro Garcés[b], Fedérico M. Serra[c]

[a] Universidad Tecnológica de Bolívar, Cartagena, Colombia
[b] Universidad Tecnológica de Pereira, 97 – Código, 660003 Pereira, Colombia
[c] Laboratorio de Control Automático (LCA), Universidad Nacional de San Luis, Villa Mercedes, San Luis 5730, Argentina

ARTICLE INFO

Article history:
Received 20 September 2017
Received in revised form 23 November 2017
Accepted 26 January 2018
Available online xxx

Keywords:
Exact feedback linearization
Passivity-based control (PBC)
Voltage source converter (VSC)
Distributed energy resource (DER)
Supercapacitor
Stability analysis

ABSTRACT

This paper presents an exact feedback linearization control strategy for voltage source converters (VSCs) applied to the integration of distributed energy resources (DERs) in smart distribution systems and microgrids. System dynamics is represented by an average nonlinear model which is transformed algebraically into an equivalent linear model by simple substitutions, avoiding to use Taylor's series or another equivalent linearization technique. The equivalent linear model preserves all characteristics of the nonlinear model, which implies that the control laws obtained are completely applicable on its nonlinear representation. Stability analysis is made using the passivity-based technique. The exact feedback linearization control in combination with passivity-based control (PBC) theory guarantees to obtain a global asymptotically stable controller in the sense of Lyapunov for its closed-loop representation. The effectiveness and robustness of the proposed methodology is tested in a low-voltage microgrid with a photovoltaic system, a supercapacitor energy storage (SCES) device and unbalance loads. All simulation scenarios are conducted in MATLAB/SIMULINK environment via SimPowerSystem library.

1. Introduction

Distributed energy resources (DERs) have taken special relevance in electrical networks in the era of the global warming which is accelerated mainly by electrical and transportation systems [1,2]. In the case of the electrical systems, the fossil fuels used to generate electricity [3–5] can be replaced by DERs which include renewable generation (wind and solar [6–8]) as well as energy storage devices [9]. The main disadvantage of renewable generation is the high variability of the primary energy resources (solar radiation or speed of the wind) [7,10]. This disadvantage is compensated with multiple devices available in the market which allow to store some energy [9], and to support the power oscillations in order to improve efficiency, reliability and security of the grid [11].

In this context, modern electrical grids are composed by the interconnection of classical generation technologies, renewable energy resources, energy storage devices and time-varying loads as depicted in Fig. 1 [7,12–14]. This interconnection origins the concept of microgrid (MG), which allows an efficient interconnection of all aforementioned devices under grid-connected and isolated scenarios [15–18].

The integration of DERs requires the use of power electronic converters [19–22], which maximizes energy production and improves grid efficiency and stability [23,24]. In fact, the correct operation of the grid is highly dependent on the capacity of the power electronic converters to make their assigned tasks [16]. In this context, are required robust, fast and reliable control strategies that allow to operate the power electronic converters in all possible operating scenarios [25]. Despite the wide range of power electronic converters [26], we are interested in analyzing the most common and widely used device, i.e., the voltage source converter (VSC) [25]. This converter is indispensable in the conformation of ac modern electrical networks [11,16,17,27,28].

In specialized literature there exist multiple papers that analyze and propose control strategies for VSCs. The most common control strategy is the classical proportional-integral control [29], linear feedback realizations [11,30] and model predictive control [31]. These controls are typically hierarchical. This situation complicates the stability analysis, because the VSCs are analyzed by small

* Corresponding author.
E-mail addresses: omontoya@utb.edu.co (O.D. Montoya), alejandro.garces@utp.edu.co (A. Garcés), fserra@ieee.org (F.M. Serra).

https://doi.org/10.1016/j.est.2018.01.014
2352-152X/

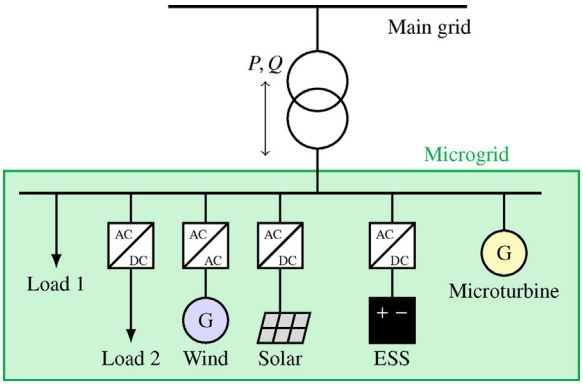

Fig. 1. Typical interconnection of DERs, which conform a MG.

subsystems, which do not necessarily imply global stability when they are interconnected.

Nonlinear control strategies can also be found to operate the VSC as is the case of passivity-based controllers [32–34] or controllers by sliding modes [35]. In these cases, the main problem lies in the calibration of the control parameters or the necessary computational time required to calculate the control signals [33]. Finally, it is also possible to find controllers based-on artificial intelligence as is the case of fuzzy logic [36,37] or artificial neural networks [38]. These strategies are efficient and simple for implementation, but lack stability demonstration. There have been also presented linear controllers, where the stability analysis has been made using passivity-based techniques [39,40]. These papers explore the possibility to design a classical PI controller via passivation theory, guaranteeing stability properties in the sense of Lyapunov.

This paper studies the nonlinear dynamical model of a VSC and its linear equivalent representation. An exact feedback linear controller to operate a grid connected VSC is proposed, and the stability analysis is made using Lyapunov theory and the passivity based technique. The fundamental difference with the existing proposals is the simplicity in the design of the control parameters and the low computational resources needed, combined with the stability properties. This is because the proposed strategy combines the advantages of linear controllers such as PI or feedback realizations and passivity based control.

The proposed control is not only stable but also passive too, which is an important property in complex and highly interconnected systems since the interconnection of two passive components is also passive [41,42]. Robustness of the methodology is demonstrated via simulation on a realistic unbalanced electrical network implemented through MATLAB/SIMULINK software. To the best of the authors' knowledge, the possibility to integrate photovoltaic systems and supercapacitor energy storage devices in microgrids using a linear equivalent representation avoiding classical linearizations has not been analyzed.

The paper is organized as follows: Section 2 presents the full dynamical model of a generic VSC using an average representation. Section 3 shows the linear controller design process, as well as, the closed stable analysis and the possibility to integrate a supercapacitor energy storage system. Section 4 presents the test system and the simulation scenarios considered. The results and computational implementation is showed in Section 5, followed by the conclusions in Section 6 and the reference list.

2. Mathematical modeling of the system

The classical topology commonly used to integrate DERs in the electrical grids using VSCs is presented in Fig. 2 [33]. Applying Kirchhoff's second law in the ac side of the VSC three ordinary

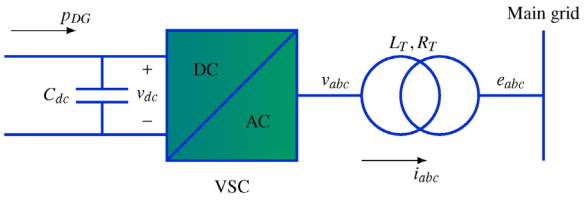

Fig. 2. Classical interconnection of a VSC for DER applications.

differential equations are obtained. These relate the ac voltage in the main grid, e_{abc}, the output ac voltage of the converter, v_{abc}, and the ac output current in the VSC, i_{abc}, as given in (1) [30].

$$L_T \frac{d}{dt} i_k = -R_T i_k + v_k - e_k, \quad \forall k \in \{a, b, c\}, \tag{1}$$

where L_T and R_T are the inductance and resistance of the three-phase transformer (this transformer can be replaced by a series RL filter), respectively.

The active power transference between both sides of the converter can be obtained applying Tellegen's theorem using the energy balance ($p_{ac} = p_{dc}$) as given (2).

$$\frac{1}{2} C_{dc} \frac{d}{dt} v_{dc}^2 = p_{DG} - \sum_{k \in \{a,b,c\}} v_k i_k, \tag{2}$$

where C_{dc} is the capacitor located in the dc side, v_{dc} is the dc voltage and p_{DG} is the active power delivered by the distributed generator connected in the dc side of the converter.

Other possible representation of the energy balance can be obtained by using the equivalent voltage grid and the technical losses produced in the electrical resistance of the transformer (commutation losses in the converter have been neglected) as defined in (3).

$$\frac{1}{2} C_{dc} \frac{d}{dt} v_{dc}^2 = p_{DG} - \sum_{k \in \{a,b,c\}} \left(e_k i_k + R_T i_k^2 \right), \tag{3}$$

To analyze the dynamic of the VSC it is possible to use continuous or discontinuous models [25,40]. The continuous model is selected considering that the switching frequency in the forced commutated devices is higher than the grid frequency. Taking into account this assumption, the output voltage of the VSC can be expressed as given in (4).

$$v_k = m_k v_{dc}, \quad \forall k \in \{a, b, c\}, \tag{4}$$

where m_k corresponds to the modulation index of the leg k in the VSC and its maximum and minimum values are limited by 1 and −1, respectively.

The set of equations presented from (1) to (4) produces two possible mathematical models for the VSC: a linear and a nonlinear formulation. The latter case has been studied in [33,34,40] using passivity based control theory, however this theory has not been applied to the former case. In this paper, a proportional exact feedback linearization controller [42] combined with passivity based technique is proposed for control the VSC.

2.1. Linear reformulation

In this case, the set of equations (1), (3) and (4) produce a linear representation under the following assumptions [30]:

A1 In (3) v_{dc}^2 is defined as a new variable z. This condition is always possible because v_{dc} never takes zero or negative values (controllability requirements of the system), which implies that the sign of the z is equal to the sign of v_{dc}.

A2 A new control input is defined in (4) as $u_k = m_k v_{dc}$.

A3 The quadratic term in (3) associated to the copper losses in the transformer can be eliminated if $\omega_0 L_T \gg R_T$ or $R_T \approx 0$, where ω_0 is the electrical frequency of the ac grid.

It is important to mention that, due v_{dc} never takes negative or zero values, $m_k = u_k/v_{dc}$ always exists and with the same sign that u_k.

After using the invariant power Park's transformation and considering the aforementioned assumptions it is obtained an equivalent linear model for the dynamical system as given from (5) to (7) [26,33].

$$L_T \frac{d}{dt} i_d = -R_T i_d - \omega L_T i_q + u_d - e_d, \tag{5}$$

$$L_T \frac{d}{dt} i_q = -R_T i_q + \omega L_T i_d + u_q - e_q, \tag{6}$$

$$\frac{1}{2} C_{dc} \frac{d}{dt} z = p_{DG} - e_d i_d - e_q i_q. \tag{7}$$

The linear mathematical model defined from (5) to (7) is represented on a canonical form given in (8) [11].

$$\dot{x} = \mathcal{A}x + \mathcal{B}u + \mathcal{E}, \tag{8}$$

where the matrices $\mathcal{A}$, $\mathcal{B}$ and the external vector perturbation $\mathcal{E}$ can be obtained by comparison between (8) and the set of equations (5) to (7).

3. Linear controller design

There are many well-known methodologies to control the linear dynamical system given in (8). A methodology based on proportional feedback linearization technique is proposed in this paper. The main idea is to apply the feedback linearization technique to obtain an equivalent linear controller. The stability analysis of the resulting closed-loop dynamical system is made through passivity-based theory. The latter is important for interconnected systems where multiple controls interact simultaneously. The characteristics of passive systems are widely documented in the literature (see for example [43,41]), for the sake of completeness a brief discussion is presented in A.

The main control objectives for a VSC used in MG applications are the following:

- To control the dc voltage in terminals of the capacitor, this is, $v_{dc} \to v_{dc}^{nom}$.
- To control the reactive power interchange between the converter and the main grid.
- To maximize the active power transference between the distributed energy resource and main grid, $p_{ac} \to p_{DG}$.

Notice that the dynamical system is under-actuated, for this reason it is only possible to control two state variables at the same time [25]. In this case v_{dc} and i_q are selected as interest variables for the proposed control strategy.

3.1. Active and reactive power behavior

Active and reactive power behavior in dq reference frame can be decoupled as given in (9) [30].

$$\begin{aligned} p_{ac} &= e_d i_d, \\ q_{ac} &= -e_d i_q. \end{aligned} \tag{9}$$

A classical phase-locked loop (PLL) is used to measure the electrical frequency in the main grid [44]. From (9) it is clear that active power can be controlled selecting an adequate reference for i_d and reactive power can be controlled through i_q. Notice that it is not possible to control v_{dc} and i_d at the same time because there is a strong dependence between these two variables as can be seen in (3).

3.2. Steps to design the linear controller

To obtain the control expressions for the dynamical model presented from (5) to (7) the following procedure is applied:

- From (6) u_q is used to eliminate the dependence of i_q current on the other state variables, then it is included a damping coefficient that allows to carry i_q current to its reference.
- From (7) is obtained the reference value for i_d current through elimination of nonlinearities and including a damping coefficient that permits to improve the reference value for z.
- In (5) u_d is used to eliminate the dependence of i_d current on the other state variables, then it is added a damping coefficient that allows to carry i_d current to the reference defined in the previous step.

After applying this procedure, the control inputs u_d, u_q and i_d^{ref} are defined as (10)–(12).

$$u_d = R_T i_d + \omega L_T i_q + e_d - R_d\left(i_d - i_d^{ref}\right), \tag{10}$$

$$u_q = R_T i_q - \omega L_T i_d + e_q - R_q\left(i_q - i_q^{ref}\right), \tag{11}$$

$$i_d^{ref} = e_d^{-1}\left(p_{DG} - e_q i_q + R_{dc}^P\left(z - z^{ref}\right)\right), \tag{12}$$

where z^{ref} is the reference of the z state variable and corresponds to the square reference of the dc voltage in the supercapacitor. Additionally, the PLL system guarantees that e_d never goes to zero under normal operating conditions, which implies that (12) never goes to infinity.

3.3. Closed-loop stable analysis

The control inputs are supposed as general nonlinear functions of the state variables $m_d = \alpha(x)$ and $m_q = \beta(x)$, such that closed-loop dynamical system takes the passivity form analyzed in (A.1) of Appendix A.

By substituting control inputs defined by (10) and (11), and i_d^{ref} presented in (12) in the linear dynamical model (see Eqs. (5)–(7)) and rearrange some terms (13) is obtained.

$$\begin{aligned} L_T \frac{d}{dt} i_d &= -R_d\left(i_d - i_d^{ref}\right), \\ L_T \frac{d}{dt} i_q &= -R_q\left(i_q - i_q^{ref}\right), \\ \frac{1}{2} C_{dc} \frac{d}{dt} z &= -R_{dc}^P\left(z - z^{ref}\right). \end{aligned} \tag{13}$$

In (13), by defining four new stable variables and considering the reference values as constant values, it is easy to transform this set of equations into (14).

$$\begin{aligned} L_T \frac{d}{dt} y_1 &= -R_d y_1, \\ L_T \frac{d}{dt} y_2 &= -R_q y_2, \\ \frac{1}{2} C_{dc} \frac{d}{dt} y_3 &= -R_{dc}^P y_3. \end{aligned} \tag{14}$$

Notice that rearranging some terms in (14) is possible to obtain a Hamiltonian formulation in closed-loop for the nonlinear system as function of y variables, as given in (15) [45].

$$\begin{pmatrix} \dot{y}_1 \\ \dot{y}_2 \\ \dot{y}_3 \end{pmatrix} = -\begin{bmatrix} L_T^{-1}R_d & 0 & 0 \\ 0 & L_T^{-1}R_d & 0 \\ 0 & 0 & 2C_{dc}^{-1}R_{dc}^{P} \end{bmatrix} \begin{pmatrix} y_1 \\ y_2 \\ y_3 \end{pmatrix}. \tag{15}$$

Global asymptotically stability conditions are guaranteed if $\mathcal{R}_{\mathcal{D}}$ is positive definite and $\mathcal{H}_{\mathcal{D}}(y)$ fulfill Lyapunov conditions as it will be explained in A. In this case $\mathcal{H}_{\mathcal{D}}(y)$ is a positive hyperboloid function in fourth dimension with vertex at the origin of the coordinates. For this reason, it is only necessary to guarantee that $\mathcal{R}_{\mathcal{D}}$ be positive definite, which is totally evident in (15).

The solution space to guarantee globally asymptotically stability in closed-loop in the sense of Lyapunov is presented below:

$$\mathcal{S}: \left\{R_d, R_q, R_{dc}^{P}\right\} \in R^{+}. \tag{16}$$

3.4. Supercapacitor energy storage application

The proposed linear control can be applied to control SCES systems easily [46]. In case of this application it is not possible to control active and reactive power interchange and, at the same time, control the voltage in the supercapacitor device [15,47]. For this reason, the control strategy on a SCES system requires the following steps:

- Use control inputs (10) and (11), in order to control active and reactive power independently (refers to (9)) via direct and quadrature currents, respectively. The reference for the direct and quadrature axis current are defined as follows:

$$i_d^{ref} = e_d^{-1} p_{ac}^{ref}, \tag{17}$$

$$i_q^{ref} = -e_d^{-1} q_{ac}^{ref}. \tag{18}$$

- To control active power interchange, the desired direct current reference is defined as (17) taking into account that the energy storage variable ($v_{dc} \leftrightarrow \sqrt{z}$) is limited by maximum and minimum values as is presented in Fig. 3.

In Fig. 3 is depicted the dynamical behavior of the energy stored in a supercapacitor device. In this picture there exist three critical points called A, B and C, respectively. The point A shows the minimum voltage value permissible for the supercapacitor terminals ($v_{dc}^{\min}$) that origins the admissible minimum energy stored value ($E_{\min}$); this voltage value corresponds to the lower bound in the SCES operation to guarantee controllability of the closed loop system. On the other hand, point C corresponds to the upper bound of the energy storage variable, which yields the maximum energy stored permissible in the supercapacitor device ($v_{dc}^{\max} \leftrightarrow E_{\max}$). While point B represents some operating point between A and C.

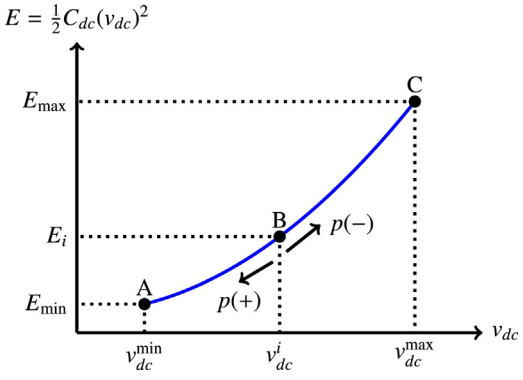

Fig. 3. Energy stored behavior in the supercapacitor device.

Notice that point B allows to have positive or negative active power reference. In case p takes positive values, the energy stored decreases carrying point B to point A. In case p takes negative values, the energy stored increases carrying point B to point C. It is important to mention that in case of point A, the active power reference only can take negative (or zero) values to increase (or hold) the total energy stored in the supercapacitor; while in the case of point C the active power reference only can take positive (or zero) values to decrease (or hold) the total energy stored in the supercapacitor device.

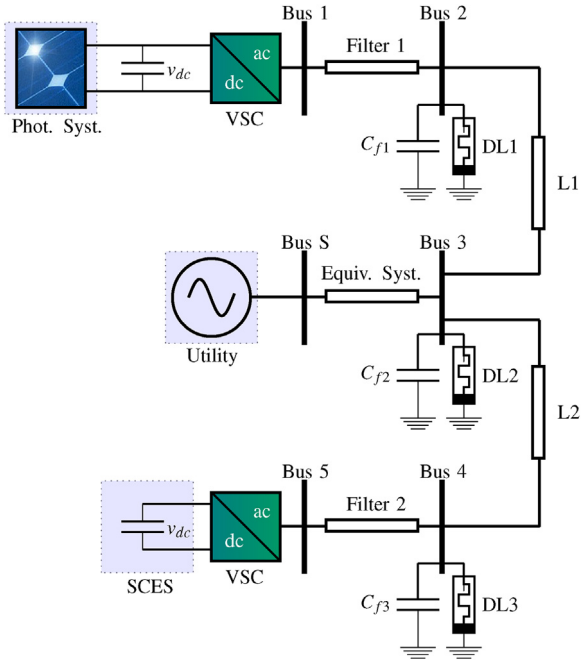

Fig. 4. Test system configuration.

Table 1
Electrical parameters of the microgrid.

Parameter	Value	Unit
DC voltage at the Phot. Syst.	800	V
DC voltage at the SCES Syst.	1500	V
Capacitance at the Phot. Syst.	0.5	F
Capacitance at the SCES Syst.	1	F
Capacitance at the bus 1	200	μF
Capacitance at the bus 2	150	μF
Capacitance at the bus 3	200	μF
Filter 1 inductance	800	μH
Filter 2 inductance	800	μH
Filter 1 resistance	50	mΩ
Filter 2 resistance	50	mΩ
Grid voltage, line to line, rms	380	V
Grid fundamental frequency	50	Hz
Line 1 inductance	100	μH
Line 2 inductance	120	μH
Line 1 resistance	50	mΩ
Line 2 resistance	60	mΩ
Equiv. Syst. inductance	200	μH
Equiv. Syst. resistance	20	mΩ

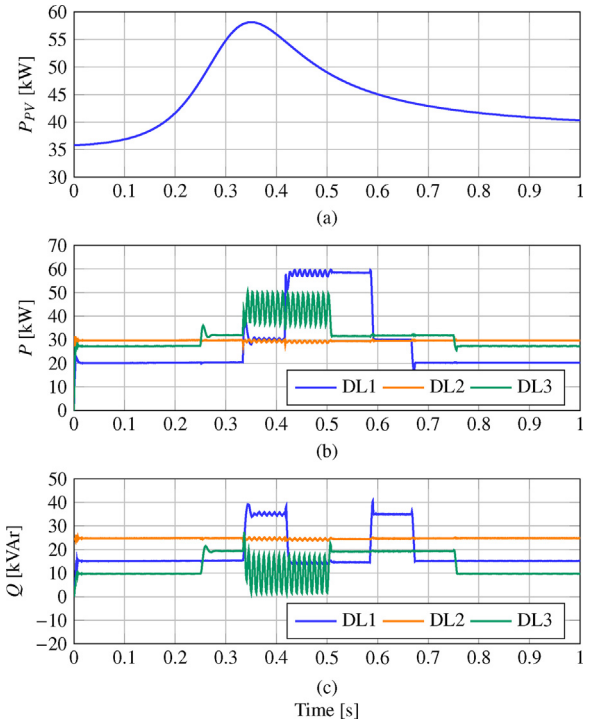

Fig. 5. Active and reactive power consumed/generated in the dynamic loads and photovoltaic generation: (a) available power generation in the photovoltaic generation system, (b) active power consumption in the dynamic loads and (c) reactive power consumption in the dynamic loads.

4. Test system and simulation cases

This section presents the general information related to the test system and simulation cases.

4.1. Test system

As test system a low voltage microgrid is employed, its configuration is depicted in Fig. 4. All parameters of this system are presented in Table 1. These values have been taken from [14].

The information related to total active power available in the photovoltaic system is presented in Fig. 5a; while active and reactive power behavior of dynamic loads are depicted in Fig. 5b and c, respectively.

Notice that for DL3 there are balanced and unbalanced loads, which produces oscillations in the normal operation of the microgrid.

4.2. Simulation cases

To evaluate the performance and capacity of the linear proposed controller two simulation cases are employed as follows:

- Case 1: In the photovoltaic system, the generic converter is controlled to transfer all active power available in the dc side at the same time that supports all reactive power required by the dynamic load 1.
- Case 2: The SCES system is employed to support all reactive power requirements in the dynamic load 3. This SCES is also used to reduce active power oscillations caused by unbalance load conditions in this load.

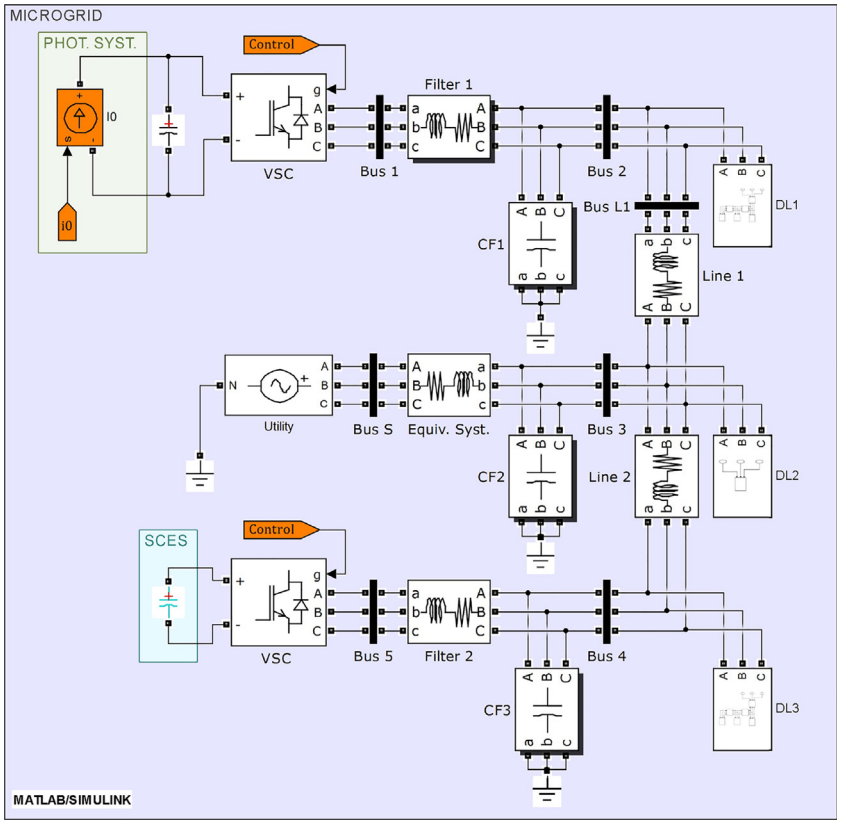

Fig. 6. MATLAB/SIMULINK implementation of the microgrid presented in Fig. 4.

5. Computational implementation and results

To evaluate the proportional feedback linearization controller proposed in this paper simulation results are presented. All simulation scenarios are conducted in MATLAB/SIMULINK using the SimPowerSystem library. Fig. 6 shows the system used in the simulation tests.

Notice that in Fig. 6, the photovoltaic system has been modeled as controlled current source. The control input is $i_{GD} = P_{GD}/v_{dc}$ as presented in Fig. 2, where P_{GD} corresponds to the active power available in the dc side. The power curve has been selected arbitrarily to demonstrate the robustness of the methodology proposed.

On the other hand, in Fig. 7 are given the controller diagrams as well as the references calculation for the PV and SCES systems, respectively. Notice that, in case of the PV system, the direct and quadrature current references are calculated as given in (10) and (17). In case of SCES system the quadrature current reference is calculated in the same form used in the PV case, this is, by using (17); nevertheless, in case of the direct current reference to guarantee the maximum and minimum state of charges allowed in the operation of the supercapacitor, a system with logic gates is used, as defined by Fig. 3.

In the parametrization of the controllers for the PV and SCES systems, we use the following values: $R_d = R_q = R_{dc} = 1 \times 10^3$; additionally, the switching frequency employed for PWM was fixed in 10 kHz.

5.1. Case 1

This simulation scenario evaluates the possibility that the VSC holds the dc voltage in the capacitor in a constant value, in order to transfer all active power available in the photovoltaic system to ac grid. Besides, the converter is used to support all reactive power demanded by DL1. In Fig. 8 are presented the active power transferred from the photovoltaic system to the ac side as well as the steady state error, the dc-link voltage and the power factor in the dynamic load before and after the compensation.

5.2. Case 2

In this simulation scenario is evaluated the capacity to use a SCES system to compensate the power oscillations caused by the unbalance behavior in the DL3. The possibility of compensating all reactive power demanded by DL3 is also evaluated. Fig. 9 shows the active and reactive power in DL3 after compensation as well as the voltage behavior in the supercapacitor.

The SCES system guarantees the unity power factor in dynamic load 3 at the same time that its active power oscillations are reduced considering an average consumption in this load around 30 kW.

5.3. Results analysis

After evaluating the dynamic performance of the proposed controller, it is possible to affirm:

- The tracking error, between the total active power available in the photovoltaic system (dc link) and the active power in the ac side of the converter is 2% of averaged value with oscillations of the 2%, caused mainly by the unbalanced loads as can be seen in Fig. 8b. Additionally, there appear commutation losses in the converter and the resistance of the filter, which are not quantified. This power loss affects the tracking reference process, reducing the electrical efficiency of the system.

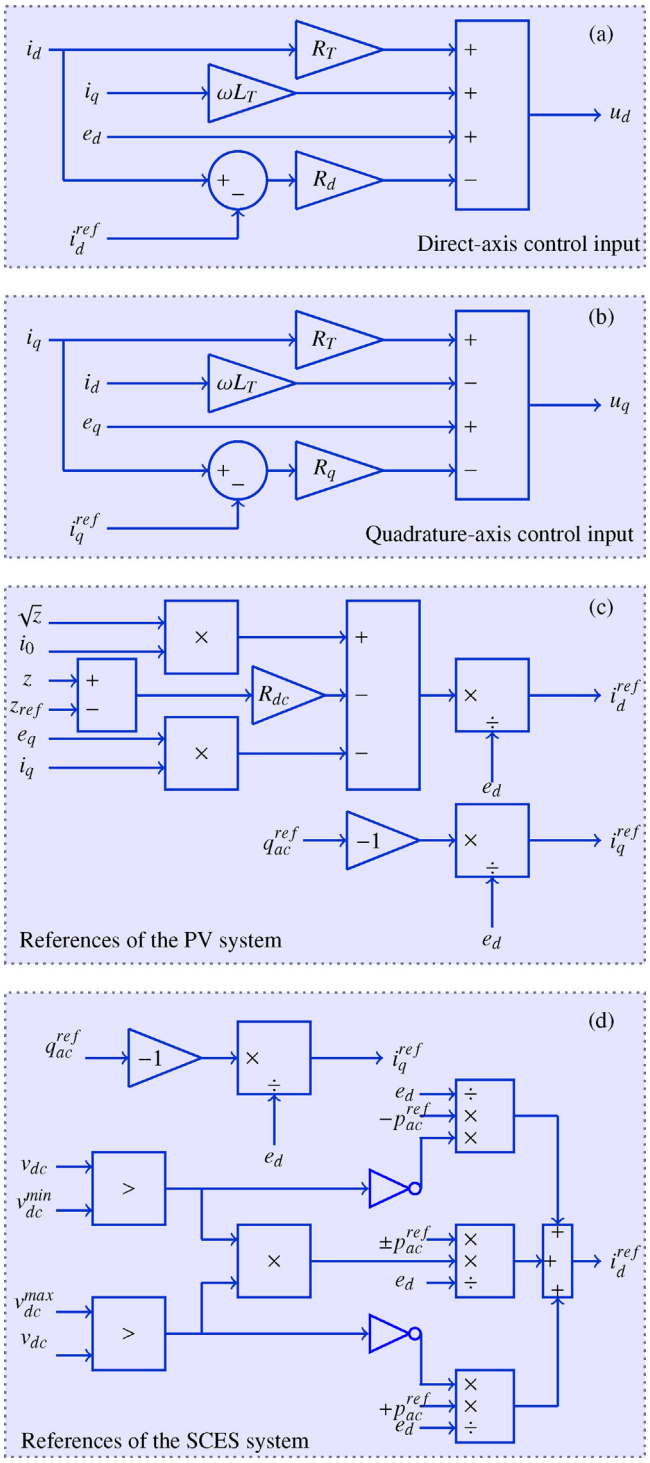

Fig. 7. PV and SCES control diagrams: (a) direct-axis control input (10), (b) quadrature-axis control input (11), (c) PV current references (12) and (18), and (d) SCES current references (17) and (18).

- The dc link voltage during simulation time always remains in this nominal value as shown in Fig. 8c, which implies that the controller fulfills the control task, delivering all active power available in the photovoltaic system holding the dc voltage as constant as possible.
- It is possible to use the VSC to support the reactive power consumed by the dynamic load as presented in Fig. 8d. Note that for all simulation time, the active power factor observed by the

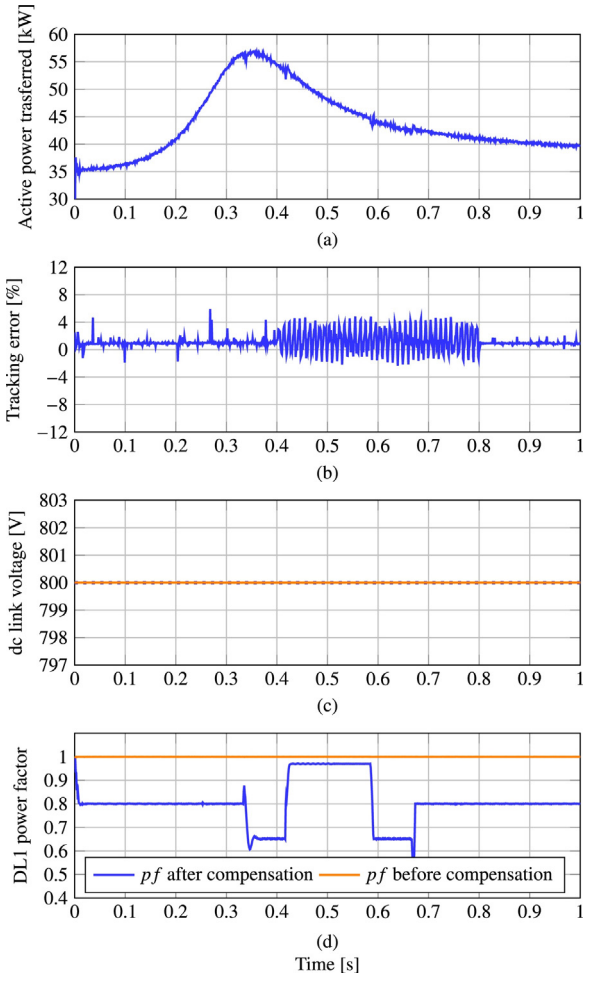

Fig. 8. Dynamical behavior in the photovoltaic and DL1 systems: (a) active power transfered from the photovoltaic system to ac system through VSC1, (b) steady state error between dc and ac power in the VSC1, (c) dc link voltage and (d) power factor in DL1 before and after compensation.

electric grid in the point of connection of DL1 is unitary as well as in DL3.

- Fig. 9c evidences that the dynamical behavior of the voltage profile in the supercapacitor device depends exclusively of the active power delivered or consumed to or from the ac grid. In this context, when the active power is positive, the supercapacitor is comporting as power generator, which implies its discharging (reduction in this voltage value), in contrast, if the active power is negative, the supercapacitor is comporting as load (increasing the voltage magnitude). This behavior is easy to observe by comparing Fig. 9b and c.

5.4. Complementary analysis

In Fig. 10 the three-phase ac voltage at the point of common coupling of the converters and the ac currents through the filters are depicted, respectively. Notice that in case of voltage profiles (see Fig. 10a and b), they have high oscillations in the first part of the simulation, but these correspond to transitory phenomena caused by the initialization of the whole electrical system. When this transitory behavior disappears, the voltage profiles have a high quality sinusoidal performance with total harmonic distortion (THD) less that 0.5%.

In case of ac current through the filters (see Fig. 10c and d), they present the same transitory phenomena at the first part of the

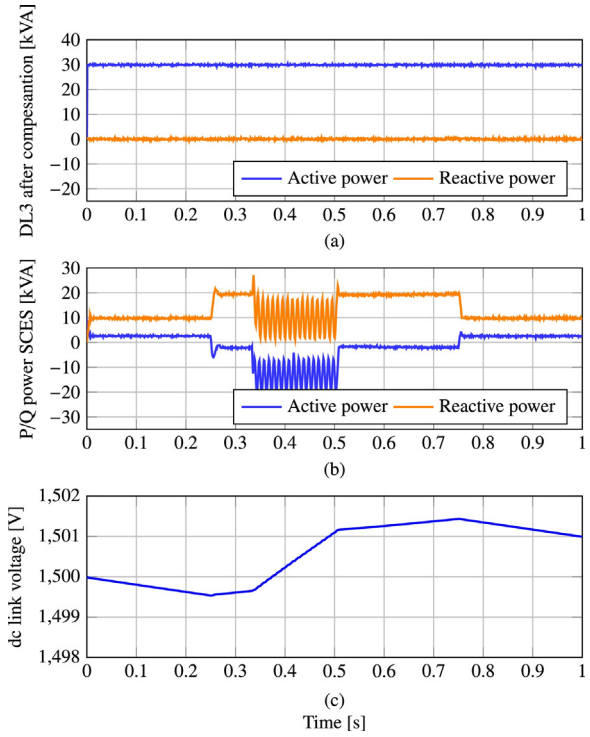

Fig. 9. Dynamical behavior in the SCES system: (a) active and reactive power consumed in DL3 after compensation, (b) active and reactive power behavior in the SCES system and (c) dc voltage in the supercapacitor device.

simulation. Notice that in case of photovoltaic system, its ac current has a better sinusoidal performance, than the case of SCES system. This behavior is caused because in the photovoltaic system the magnitude of the ac current is grater than in the SCES system, since the photovoltaic system extracts the total active power available in the panel system at the same time that compensates all reactive power demanded in DL1, while the SCES system compensates all reactive power consumed by DL3, but only compensates the oscillating part in this load.

In this sense, the THD in the ac current of the photovoltaic system is around 0.87%, while in the case of the SCES system it is around of 3.46%. Although for both devices the THD fulfills the standard related to the operation of power electronic converters.

To compare the voltage behavior between the main grid and the points of common coupling of the PV and SCES systems their average RMS variations are presented in Fig. 11. Notice that both voltage profiles have deviations less than ±5%, which is positive in terms of regulatory polices, this is, in terms of service's quality. Additionally, in case of the PV system, in some periods of time the RMS voltage profile is greater that 1 p.u; and this occurs due to the connection of the PV system operating as power generator with variable power factor and reduced conditions in the dynamic load 1, gives the possibility to overpass the voltage profile in this point since the power flows is directed from the PV system to the main grid.

In order to compare the effectiveness and efficiency of the proposed controller in Fig. 12 are presented the active power output in the case of PV system for the methodology of control proposed in this paper as well as the IDA-PBC approach [34] and the classical PI control.

Notice that the proposed exact feedback linearization controller has identical performance when it is compared to passivity-based of classical PI approaches; nevertheless, comparing the PI and proposed controller, it is clear that our proposed methodology guarantees stability in the sense of Lyapunov, while it is not the

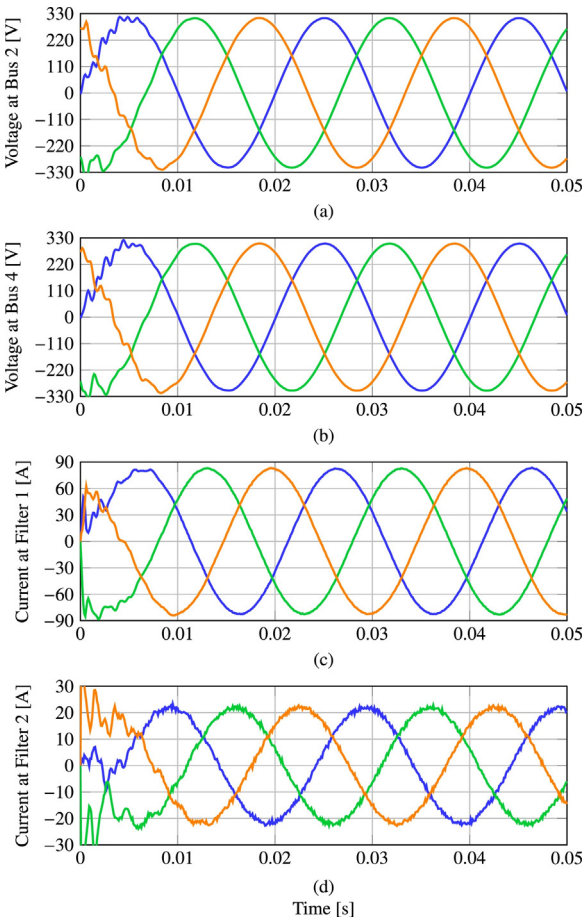

Fig. 10. Profile of the voltages and currents in the point of common coupling and series *RL* filter: (a) three-phase ac voltage at Bus 2, (b) three-phase ac voltage at Bus 4, (c) three-phase ac current through the filter 1 and (d) three-phase ac current through the filter 2.

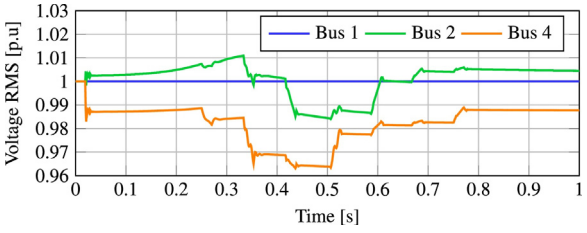

Fig. 11. Dynamical behavior of the RMS values at the main grid and the points of common coupling of the VSCs.

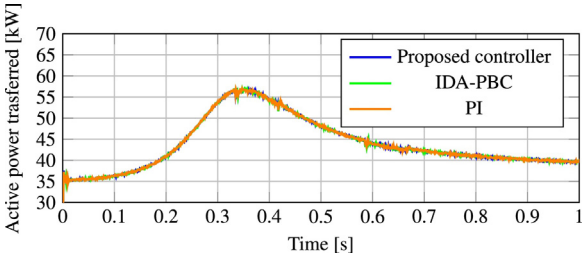

Fig. 12. Comparison between the available active power in the PV system and the output power for different control approaches.

case of the PI control. Additionally, the PBC approach corresponds to the nonlinear version of the exact feedback linearization proposed, for this reason they have the same dynamical behavior (see Ref. [33]).

6. Conclusions and future work

This paper showed the linear controller design via feedback linearization and passivity-based control theories to integrate distributed energy resources in microgrids. The main characteristic of the controller proposed is that it combines the main advantages of linear controllers, such as: PI and feedback realizations with the passivity based control theory without employing linearization techniques on the dynamical model of the VSC; since only some changes of variables are made to obtain its equivalent linear model.

The proposed controller allows to integrate multiple DERs in MGs practically without changes in its basic structure, as was evidenced in the case of the SCES application, which implies that it would be easily scalable to other distributed energy technologies based on VSC.

As future work, the electrical network could be analyzed as a whole system, exploiting its passivity properties, in order to design a unified controller to operate all devices interconnected with this via passivity-based control theory and exact feedback linearization analysis. This control approach can guarantee stable operating conditions during different operating scenarios in the electrical network.

Acknowledgements

This work was supported by the National Scholarship Program Doctorates of the Administrative Department of Science, Technology and Innovation of Colombia (COLCIENCIAS), by calling contest 727-2015, by PhD program in Engineering of the Universidad Tecnológica de Pereira, Colombia, by Universidad Nacional de San Luis, Argentina, and Consejo Nacional de Investigaciones Científicas y Técnicas (CONICET), Argentina.

Appendix A. Stability analysis of a Hamiltonian system with dissipation

Suppose that exist two vector control inputs $u_d = \alpha(x)$ and $u_q = \beta(x)$ for the nonlinear and linear models, such that generate a closed-loop desired dynamical behavior as defined in (A.1) [45,34].

$$\dot{x} = [\mathcal{J}_{\mathcal{D}} - \mathcal{R}_{\mathcal{D}}]\nabla\mathcal{H}_{\mathcal{D}}(x), \tag{A.1}$$

where $\mathcal{J}_{\mathcal{D}}$ is the antisymmetric interconnection desired matrix, $\mathcal{R}_{\mathcal{D}}$ is the positive definite desired matrix and $\mathcal{H}_{\mathcal{D}}(x)$ is the positive definite Hamiltonian function with a global minimum in the desired operative point x^* [33,40].

Notice that $\mathcal{H}_{\mathcal{D}}(x)$ can be used as candidate Lyapunov because it fulfill the first two conditions to prove stability around critical point for autonomous dynamical systems [45]. In order to prove that the dynamical systems is globally asymptotically stable in the sense of Lyapunov is just necessary to prove that $\dot{\mathcal{H}}_{\mathcal{D}}(x)$ is always negative definite. Applying the time derivative for $\mathcal{H}_{\mathcal{D}}(x)$ (A.2) is obtained.

$$\frac{d}{dt}\mathcal{H}_{\mathcal{D}}(x) = [\nabla\mathcal{H}_{\mathcal{D}}(x)]^T\dot{x}. \tag{A.2}$$

After substituting (A.1) in (A.2) it carries to (A.3).

$$\frac{d}{dt}\mathcal{H}_{\mathcal{D}}(x) = [\nabla\mathcal{H}_{\mathcal{D}}(x)]^T[\mathcal{J}_{\mathcal{D}} - \mathcal{R}_{\mathcal{D}}][\nabla\mathcal{H}_{\mathcal{D}}(x)]. \tag{A.3}$$

Since $\mathcal{J}_{\mathcal{D}}$ is antisymmetric then (A.3) can be reduced as (A.4).

$$\frac{d}{dt}\mathcal{H}_{\mathcal{D}}(x) = -[\nabla\mathcal{H}_{\mathcal{D}}(x)]^{T}[\mathcal{R}_{\mathcal{D}}][\nabla\mathcal{H}_{\mathcal{D}}(x)]. \tag{A.4}$$

If $\mathcal{R}_{\mathcal{D}}$ is positive semidefinite, then the dynamical system is stable in the sense of Lyapunov; nevertheless, if $\mathcal{R}_{\mathcal{D}}$ is positive definite, then the dynamical system is globally asymptotically stable in the sense of Lyapunov [41–43,45].

References

[1] A. Hussain, S.M. Arif, M. Aslam, Emerging renewable and sustainable energy technologies: state of the art, Renew. Sustain. Energy Rev. 71 (2017) 12–28, doi:http://dx.doi.org/10.1016/j.rser.2016.12.033.

[2] A.A. Makky, A. Alaswad, D. Gibson, A. Olabi, Renewable energy scenario and environmental aspects of soil emission measurements, Renew. Sustain. Energy Rev. 68 (2017) 1157–1173, doi:http://dx.doi.org/10.1016/j.rser.2016.05.088.

[3] S.B. Walker, D. van Lanen, U. Mukherjee, M. Fowler, Greenhouse gas emissions reductions from applications of power-to-gas in power generation, Sustain. Energy Technol. Assess. 20 (2017) 25–32, doi:http://dx.doi.org/10.1016/j.seta.2017.02.003.

[4] M. Barma, R. Saidur, S. Rahman, A. Allouhi, B. Akash, S.M. Sait, A review on boilers energy use, energy savings, and emissions reductions, Renew. Sustain. Energy Rev. 79 (2017) 970–983, doi:http://dx.doi.org/10.1016/j.rser.2017.05.187.

[5] M. Stadler, A. Siddiqui, C. Marnay, H. Aki, J. Lai, Control of greenhouse gas emissions by optimal DER technology investment and energy management in zero-net-energy buildings, Eur. Trans. Electr. Power 21 (2) (2011) 1291–1309, doi:http://dx.doi.org/10.1002/etep.418.

[6] M.D. Al-falahi, S. Jayasinghe, H. Enshaei, A review on recent size optimization methodologies for standalone solar and wind hybrid renewable energy system, Energy Convers. Manage. 143 (2017) 252–274.

[7] O. Ellabban, H. Abu-Rub, F. Blaabjerg, Renewable energy resources: current status, future prospects and their enabling technology, Renew. Sustain. Energy Rev. 39 (2014) 748–764, doi:http://dx.doi.org/10.1016/j.rser.2014.07.113.

[8] P. Shanthi, G. Uma, M.S. Keerthana, Effective power transfer scheme for a grid connected hybrid wind/photovoltaic system, IET Renew. Power Gener. 11 (7) (2017) 1005–1017, doi:http://dx.doi.org/10.1049/iet-rpg.2016.0592.

[9] S.O. Amrouche, D. Rekioua, T. Rekioua, S. Bacha, Overview of energy storage in renewable energy systems, Int. J. Hydrogen Energy 41 (45) (2016) 20914–20927.

[10] X. Li, D. Hui, X. Lai, Battery energy storage station (BESS)-based smoothing control of photovoltaic (PV) and wind power generation fluctuations, IEEE Trans. Sustain. Energy 4 (2) (2013) 464–473, doi:http://dx.doi.org/10.1109/TSTE.2013.2247428.

[11] A. Ortega, F. Milano, Generalized model of VSC-based energy storage systems for transient stability analysis, IEEE Trans. Power Syst. 31 (5) (2016) 3369–3380, doi:http://dx.doi.org/10.1109/TPWRS.2015.2496217.

[12] A. Kaur, J. Kaushal, P. Basak, A review on microgrid central controller, Renew. Sustain. Energy Rev. 55 (2016) 338–345, doi:http://dx.doi.org/10.1016/j.rser.2015.10.141.

[13] M.S. Mahmoud, M.S.U. Rahman, F.M.A.L. Sunni, Review of microgrid architectures: a system of systems perspective, IET Renew. Power Gener. 9 (8) (2015) 1064–1078, doi:http://dx.doi.org/10.1049/iet-rpg.2014.0171.

[14] M.M. Rezaei, J. Soltani, A robust control strategy for a grid-connected multi-bus microgrid under unbalanced load conditions, Int. J. Electr. Power Energy Syst. 71 (2015) 68–76. http://www.sciencedirect.com/science/article/pii/S0142061515001246.

[15] H.F. Habib, A. Mohamed, M.E. Hariri, O.A. Mohammed, Utilizing supercapacitors for resiliency enhancements and adaptive microgrid protection against communication failures, Electr. Power Syst. Res. 145 (2017) 223–233.

[16] S. Parhizi, H. Lotfi, A. Khodaei, S. Bahramirad, State of the art in research on microgrids: a review, IEEE Access 3 (2015) 890–925, doi:http://dx.doi.org/10.1109/ACCESS.2015.2443119.

[17] K. Rajesh, S. Dash, R. Rajagopal, R. Sridhar, A review on control of ac microgrid, Renew. Sustain. Energy Rev. 71 (2017) 814–819, doi:http://dx.doi.org/10.1016/j.rser.2016.12.106.

[18] U.B. Tayab, M.A.B. Roslan, L.J. Hwai, M. Kashif, A review of droop control techniques for microgrid, Renew. Sustain. Energy Rev. 76 (2017) 717–727, doi:http://dx.doi.org/10.1016/j.rser.2017.03.028.

[19] P. Szcześniak, J. Kaniewski, Power electronics converters without dc energy storage in the future electrical power network, Electr. Power Syst. Res. 129 (2015) 194–207.

[20] A. Ortega, F. Milano, Modeling, simulation, and comparison of control techniques for energy storage systems, IEEE Trans. Power Syst. 32 (3) (2017) 2445–2454, doi:http://dx.doi.org/10.1109/TPWRS.2016.2602211.

[21] B. Badrzadeh, Power conversion systems for modern ac-dc power systems, Eur. Trans. Electr. Power 22 (7) (2012) 879–906, doi:http://dx.doi.org/10.1002/etep.611.

[22] R. Hemmati, N. Azizi, Optimal control strategy on battery storage systems for decoupled active-reactive power control and damping oscillations, J. Energy Storage 13 (Supplement C) (2017) 24–34, doi:http://dx.doi.org/10.1016/j.est.2017.06.003.

[23] J. Rocabert, A. Luna, F. Blaabjerg, P. Rodríguez, Control of power converters in AC microgrids, IEEE Trans. Power Electron. 27 (11) (2012) 4734–4749, doi:http://dx.doi.org/10.1109/TPEL.2012.2199334.

[24] O. Palizban, K. Kauhaniemi, Distributed cooperative control of battery energy storage system in ac microgrid applications, J. Energy Storage 3 (Suppl. C) (2015) 43–51, doi:http://dx.doi.org/10.1016/j.est.2015.08.005.

[25] R. Teodorescu, M. Liserre, P. Rodriguez, Grid Converters for Photovoltaic and Wind Power Systems, Wiley – IEEE, 2011.

[26] M.H. Ali, B. Wu, R.A. Dougal, An overview of SMES applications in power and energy systems, IEEE Trans. Sustain. Energy 1 (1) (2010) 38–47, doi:http://dx.doi.org/10.1109/TSTE.2010.2044901.

[27] E. Planas, J. Andreu, J.I. Gárate, I. Martínez De Alegría, E. Ibarra, AC and DC technology in microgrids: a review, Renew. Sustain. Energy Rev. 43 (2015) 726–749, doi:http://dx.doi.org/10.1016/j.rser.2014.11.067.

[28] F. Zhang, H. Zhao, M. Hong, Operation of networked microgrids in a distribution system, CSEE J. Power Energy Syst. 1 (4) (2015) 12–21.

[29] A. Rahim, E. Nowicki, Supercapacitor energy storage system for fault ride-through of a {DFIG} wind generation system, Energy Convers. Manage. 59 (2012) 96–102.

[30] J. Shi, Y. Tang, K. Yang, L. Chen, L. Ren, J. Li, S. Cheng, SMES based dynamic voltage restorer for voltage fluctuations compensation, IEEE Trans. Appl. Supercond. 20 (3) (2010) 1360–1364, doi:http://dx.doi.org/10.1109/TASC.2010.2041499.

[31] J. Binkai, W. Zhixin, Z. Jianlong, S. Li, Study on an improved model predictive control strategy with power self-coordination for VSC-MTDC, Energy Procedia 100 (2016) 261–265 3rd International Conference on Power and Energy Systems Engineering, CPESE 2016, 8–10 September 2016, Kitakyushu, Japan.

[32] X. Fan, L. Guan, C. Xia, T. Ji, IDA-PB control design for VSC-HVDC transmission based on PCHD model, Int. Trans. Electr. Energy Syst. 25 (10) (2015) 2133–2143, doi:http://dx.doi.org/10.1002/etep.1953 eTEP-13-0141.R1.

[33] F.M. Serra, C.H.D. Angelo, IDA-PBC controller design for grid connected front end converters under non-ideal grid conditions, Electr. Power Syst. Res. 142 (2017) 12–19.

[34] F.M. Serra, C.H.D. Angelo, D.G. Forchetti, Interconnection and damping assignment control of a three-phase front end converter, Int. J. Electr. Power Energy Syst. 60 (2014) 317–324.

[35] S. Dhar, P. Dash, A new backstepping finite time sliding mode control of grid connected PV system using multivariable dynamic VSC model, Int. J. Electr. Power Energy Syst. 82 (2016) 314–330.

[36] S.S. Khorramabadi, A. Bakhshai, Critic-based self-tuning pi structure for active and reactive power control of VSCs in microgrid systems, IEEE Trans. Smart Grid 6 (1) (2015) 92–103, doi:http://dx.doi.org/10.1109/TSG.2014.2354651.

[37] D. Amoozegar, DSTATCOM modelling for voltage stability with fuzzy logic PI current controller, Int. J. Electr. Power Energy Syst. 76 (2016) 129–135, doi:http://dx.doi.org/10.1016/j.ijepes.2015.09.017.

[38] B. Singh, D.T. Shahani, A.K. Verma, Neural network controlled grid interfaced solar photovoltaic power generation, IET Power Electron. 7 (3) (2014) 614–626, doi:http://dx.doi.org/10.1049/iet-pel.2013.0166.

[39] F. Valenciaga, P.F. Puleston, P.E. Battaiotto, R.J. Mantz, Passivity/sliding mode control of a stand-alone hybrid generation system, IEE Proc. Control Theory Appl. 147 (6) (2000) 680–686, doi:http://dx.doi.org/10.1049/ip-cta:20000803.

[40] M. Perez, R. Ortega, J.R. Espinoza, Passivity-based PI control of switched power converters, IEEE Trans. Control Syst. Technol. 12 (6) (2004) 881–890, doi:http://dx.doi.org/10.1109/TCST.2004.833628.

[41] H. Khalil, Nonlinear Systems, Always Learning, Pearson Education, Limited, 2013.

[42] J. Slotine, W. Li, Applied Nonlinear Control, Prentice-Hall International Editions, Prentice-Hall, 1991.

[43] W. Haddad, V. Chellaboina, Nonlinear Dynamical Systems and Control: A Lyapunov-Based Approach, Princeton University Press, 2011.

[44] S. Golestan, J.M. Guerrero, J.C. Vasquez, Three-phase PLLs: a review of recent advances, IEEE Trans. Power Electron. 32 (3) (2017) 1894–1907, doi:http://dx.doi.org/10.1109/TPEL.2016.2565642.

[45] S.P. Nageshrao, G.A.D. Lopes, D. Jeltsema, R. Babuska, Port-Hamiltonian systems in adaptive and learning control: a survey, IEEE Trans. Autom. Control 61 (5) (2016) 1223–1238, doi:http://dx.doi.org/10.1109/TAC.2015.2458491.

[46] H. Spth, K.-P. Becker, Energy storage by capacitors, Eur. Trans. Electr. Power 12 (3) (2002) 211–216, doi:http://dx.doi.org/10.1002/etep.4450120307.

[47] O. Palizban, K. Kauhaniemi, Energy storage systems in modern grids-matrix of technologies and applications, J. Energy Storage 6 (Suppl. C) (2016) 248–259, doi:http://dx.doi.org/10.1016/j.est.2016.02.001.